


Magnetoelectric coupling and cross control in two-dimensional ferromagnets

Fan Wang,^{1,†} Ying Zhou,^{2,†} Xiaofan Shen,³ Shuai Dong^{1,2} and Juntong Zhang^{1,*}

¹*School of Materials Science and Physics, China University of Mining and Technology, Xuzhou 221116, China*

²*School of Physics, Southeast University, Nanjing 211189, China*

³*National Laboratory of Solid State Microstructures and Physics School, Nanjing University, Nanjing 210093, China*

 (Received 6 May 2023; revised 3 November 2023; accepted 20 November 2023; published 7 December 2023)

The coexistence and coupling of multiple ferroics may not only cause some novel physical phenomena but also provide new means for the detection and control of electronic degrees of freedom. In recent years, two-dimensional (2D) ferroelectricity and ferromagnetism have been experimentally confirmed in van der Waals materials but their coexistence and coupling have rarely been demonstrated in single-phase materials. Here, a general mechanism for the coexistence and coupling of three ferroics has been demonstrated in van der Waals monolayer ferromagnets lacking inversion symmetry, in which spin-orbit coupling leads to spin-direction-dependent ferroelectricity and ferrovalley. This causes the emergence of some interesting phenomena, such as the anomalous valley Hall effect without an applied electric field. The ferroelectric polarization induced in a 2D ferromagnet with strong spin-orbit coupling can be close to the largest known spin-induced polarization. Importantly, the magnetoelectric coupling effect enables the cross control of ferroic order parameters by external fields, such as controlling magnetization by an electric field and polarization by a magnetic field.

DOI: [10.1103/PhysRevApplied.20.064011](https://doi.org/10.1103/PhysRevApplied.20.064011)

I. INTRODUCTION

Finding new ways to manipulate electrons has become a key challenge in the development of next-generation electronic devices with high density, high processing speed, multifunctionality, and low energy consumption [1–5]. The detection and control of electrons are often inseparable from their inherent degrees of freedom [1–3]. Besides charge and spin, electrons have another novel degree of freedom in the momentum space of the crystal, the valley, which has been proposed as a potential information carrier [6]. The coupling between different electronic degrees of freedom can not only cause some novel physical phenomena such as the quantum anomalous Hall effect and the valley Hall effect but also enable the cross control of electronic degrees of freedom by external fields, which is of great significance for the development of spintronics and valleytronics [7–13].

Two-dimensional (2D) ferroelectricity and ferromagnetism, rooted in charge and spin degrees of freedom, respectively, have recently been demonstrated in van der Waals materials [14–19]. In addition, the concept of ferrovalley with spontaneous valley polarization has also

been proposed in 2D materials [8,20]. Since then, the coexistence and coupling of multiple ferroics in single-phase 2D materials has attracted increasing interest [21–25]. From the perspective of symmetry, ferroelectricity and ferrovalley require the breaking of spatial-inversion symmetry, while ferromagnetism breaks time-inversion symmetry. 2D ferromagnetism also requires spin-orbit coupling (SOC) to remove the restriction of the 2D isotropic Heisenberg model on the emergence of long-range magnetic order [26]. SOC is known to cause a variety of fascinating physical phenomena in nonmagnetic crystals lacking an inversion center, such as inducing momentum-dependent effective magnetic fields and leading to spin-valley locking [7,27]. In 2D magnetically ordered materials, the combination of inversion symmetry breaking and SOC may also cause some novel effects [11,28].

In this work, we demonstrate the spin-direction-dependent ferroelectric and valley polarization caused by SOC in 2D ferromagnets lacking inversion symmetry, as well as the magnetoelectric cross-control effects, by combining symmetry analysis, first-principles calculations, and Monte Carlo and atomistic spin-dynamics simulations. We explain the microscopic mechanism of the discovered spin-induced ferroelectricity and reveal the rules of spin-polarization coupling and spin-valley coupling. We show that not only the coexistence and coupling of multiple ferroics but also the control of various ferroic order

*juntongzhang@cumt.edu.cn

†These authors contributed equally to this work.

parameters by external fields can be realized in the monolayer system.

II. COMPUTATIONAL DETAILS

The first-principles calculations based on density-functional theory (DFT) were performed using the projector-augmented-wave (PAW) method [29], as implemented in the Vienna *ab initio* simulation package (VASP) [30]. The Perdew-Burke-Ernzerhof functional was used as the exchange-correlation functional and the Hubbard- U method within the rotationally invariant formalism was used to treat the electron correlation in the d shell of transition-metal ions [31]. The effective values of $U_{\text{eff}} = 2.1, 1.5, 0.6$ eV for the d electrons of the VSe_2 , VTe_2 , and RuBr_2 monolayers, respectively, were determined by self-consistent calculation based on the constrained random-phase approximate method [32]. For each monolayer, a vacuum space of 20 Å was used to separate the neighboring images along the vertical direction due to the periodic condition. A plane-wave cutoff energy of 600 eV was used for the plane-wave expansion and a convergence threshold of 10^{-7} eV was used for the electronic self-consistency loop. A Γ -centered $15 \times 15 \times 1$ k -point mesh was used for the Brillouin-zone integration. The in-plane (IP) lattice constants and internal atomic coordinates were relaxed until the Hellman-Feynman force on each atom was less than 5×10^{-3} eV/Å. The ferroelectric polarization was calculated by using the Berry-phase method [33] and SOC was switched on in the calculations. The phonon band structures were calculated using density-functional perturbation theory. The *ab initio* molecular-dynamics simulations at 300 K were performed in a canonical ensemble using the Nosé heat-bath scheme with a simulation time over 9 ps and a time step of 3 fs.

The Monte Carlo simulations were performed to verify the magnetic ground state and estimate the magnetic transition temperature. The Heisenberg spin model with a magnetic anisotropy term was adopted and a 64×64 spin lattice with periodic boundary conditions and the annealing algorithm were used in the simulations. For each temperature, 5×10^5 steps were taken to reach equilibrium and 10^6 steps were performed for sampling by using the Metropolis algorithm.

The atomistic spin dynamics were studied by solving the Landau-Lifshitz-Gilbert (LLG) equation [34],

$$\frac{\partial \mathbf{S}_i}{\partial t} = -\frac{\gamma}{1 + \lambda^2} [\mathbf{S}_i \times \mathbf{H}_{\text{eff}}^i + \lambda \mathbf{S}_i \times (\mathbf{S}_i \times \mathbf{H}_{\text{eff}}^i)], \quad (1)$$

where γ is the gyromagnetic ratio and λ represents the Gilbert damping constant and is set to 0.5. $\mathbf{H}_{\text{eff}}^i$ is the effective magnetic field on each spin, which can be obtained from the negative first derivative of the spin Hamiltonian,

$$\mathbf{H}_{\text{eff}}^i = -\frac{1}{\mu_S} \frac{\partial H}{\partial \mathbf{S}_i}, \quad (2)$$

where μ_S is the local spin moment. The LLG equation was solved using Heun's method with a time step of 1 fs.

III. RESULTS AND DISCUSSION

A. Spin-induced ferroelectricity in 2D ferromagnets

The invariance of spin orientation under spatial inversion prohibits the emergence of spin-induced ferroelectricity in ferromagnets with an inversion center, so spin-induced ferroelectricity usually requires a complex antiferromagnetic structure to break the inversion symmetry [35,36]. However, in ferromagnets lacking an inversion center, a single spin acting as an axial vector due to SOC can break the rotation and mirror symmetry, which may cause the nonpolar symmetry to change to a polar symmetry [23]. Thus, in principle, spin-induced ferroelectricity can occur in ferromagnets lacking an inversion center.

Most of the 2D ferromagnets discovered so far have spatial-inversion symmetry [37]. The monolayer of $2H$ -phase VSe_2 is one of the few 2D ferromagnets that have been experimentally confirmed to lack an inversion center [38]. It forms a trigonal prismatic coordination and has a nonpolar point group D_{3h} [Fig. 1(a)]. We first determined its spin-direction-dependent magnetic symmetry. When the spin direction is along a twofold rotation axis (x axis), this rotation axis and the two mirror planes parallel to this rotation axis are retained, resulting in a polar point group of $m'm'2$ [Fig. 1(b)]. The IP spin direction (y axis) perpendicular to this rotation axis has the same symmetry ($m'm'2$), except for the difference in time reversal. When the spin is along the general IP direction, the magnetic symmetry is further reduced to only the horizontal mirror plane m' , thus allowing the simultaneous occurrence of two IP polarization components. All symmetry operations are retained for the spin direction along the z axis. When the spin deviates from the z axis within the vertical planes parallel (x - z plane) and perpendicular (y - z plane) to the twofold axis, the magnetic symmetry changes to m' and $2'$, respectively [Figs. 1(c) and 1(d)]. The former can cause both IP and out-of-plane (OP) polarization components, while the latter only allows the polarization component along the twofold axis.

We then investigated the dependence of the spin-induced polarization on the spin direction by first-principles calculations. Consistent with the above symmetry analysis, the IP spin orientation induces two polarization components, P_x and P_y , which vary with the spin angle according to the cosine and sine functions, respectively [Fig. 1(b)]. The spin-induced polarization varies with a period of 180° due to the axial-vector property of the spin, so the polarization is reversed when the spin is rotated by 90° . When the spin lies in the x - z plane, the P_x component

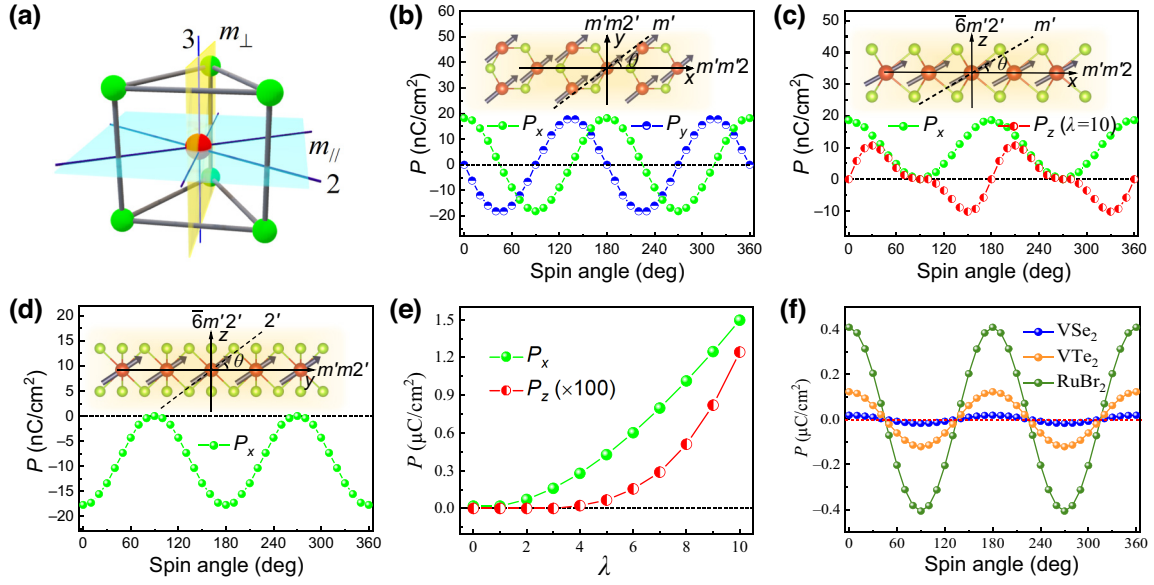


FIG. 1. The spin-direction-dependent ferroelectricity in 2D ferromagnets lacking inversion symmetry. (a) A schematic of the crystal structure and symmetry operations of the 2H-phase VSe₂ monolayer. (b)–(d) The dependence of the magnetic symmetry and the spin-induced polarization on the spin direction in the (b) *x*-*y*, (c) *x*-*z*, and (d) *y*-*z* planes, respectively. (e) The variation of the polarization components P_x and P_z with the relative strength (λ) of SOC. For comparison, the value of the P_z component is multiplied by 100. (f) The variation of the polarization component P_x with the IP spin direction for some 2D ferromagnets with the same structure (2H phase).

occurs and its sign remains unchanged but the P_z component allowed by the symmetry does not emerge within the calculation accuracy. We then increased the strength of SOC by an order of magnitude and recalculated the P_z component to verify its existence. It emerges with the enhancement of SOC, exhibiting a more complex relationship with the spin angle and reaching its maximum at approximately 30° [Fig. 1(c)]. For spin orientation in the *y*-*z* plane, only the P_x component appears and its variation with the spin angle is the same as for the *x*-*z* plane but with the opposite sign [Fig. 1(d)].

B. Mechanism of spin-induced ferroelectricity

The polarization component can be expressed as a quadratic function of the spin component according to the phenomenological model of spin-induced ferroelectricity [39–41]. For the local electric polarization induced by a single spin, it can be expressed as

$$P^\alpha = \sum_{\beta\gamma} M_{\beta\gamma}^\alpha S_\beta S_\gamma, \quad (3)$$

where α , and β and γ , represent the polarization and spin components, respectively. The form of the coefficient tensors can be determined from the local structural symmetry of the spin site. For the VSe₂ monolayer, the coefficient tensors have only one independent tensor element $M_{xx}^\alpha = -M_{yy}^\alpha = -M_{xy}^\alpha$ (for its derivation, see the Supplemental Material [42]). Then, the spin-induced polarization of the

three spin planes can be described as

$$\begin{aligned} \mathbf{P}_{xy} &= \delta(\cos 2\theta, -\sin 2\theta, 0), \\ \mathbf{P}_{xz} &= -\mathbf{P}_{yz} = \delta(\cos^2 \theta, 0, 0), \end{aligned} \quad (4)$$

where δ is proportional to the only nonzero tensor element and θ represents the spin angle. These expressions explain the calculated spin-direction dependence of the ferroelectric polarization well, except for the P_z component. That is, the general model of spin-induced ferroelectricity cannot explain the emergence of the OP polarization component.

From the perspective of microscopic origin, the spin-direction-dependent electric polarization originates from the effect of SOC on orbital hybridization. Specifically, the *p*-*d* hybridization between the magnetic ion and its ligand is modified by SOC, resulting in a change in charge transfer along each coordination bond, depending on the spin direction. The local electric polarization induced by a single spin can be described as $P \propto \sum_n (\mathbf{S} \cdot \mathbf{e}_n)^2 \mathbf{e}_n$, where \mathbf{e}_n is the unit vector connecting the magnetic ion and the *n*th ligand anion [39,43]. This mechanism has explained the dependence of the spin-induced polarization on the spin direction well in some antiferromagnets, such as Ba₂CoGe₂O₇ [44]. The polarization expressions in Eq. (4) can also be derived from this formula (see the Supplemental Material [42]). However, note that this formula is derived from the lowest-order perturbation of SOC and that the higher-order perturbation needs to be considered when the effect of the lowest-order perturbation disappears. The polarization induced by the second-order

perturbation effect of SOC can be described as $P \propto \sum_n (\mathbf{S} \cdot \mathbf{e}_n)^4 \mathbf{e}_n$. It causes an additional polarization component P_z for the x - z spin plane, which can be expressed as (see the Supplemental Material [42])

$$P_{xz}^z \propto \cos^3 \theta \sin \theta. \quad (5)$$

This polarization expression agrees well with the calculated spin-direction dependence of the OP polarization.

The magnitude of this spin-induced polarization depends on the strength of the SOC. Both the IP and OP polarization components increase significantly with the enhancement of SOC and the latter rises more sharply with the further increase of the SOC constant [Fig. 1(e)]. Therefore, this spin-induced polarization is expected to be significantly improved in 2D ferromagnets with strong SOC. We then calculated the spin-induced polarization of some other 2D ferromagnets, including VTe₂ and RuBr₂ monolayers, which have the same structure as the VSe₂ monolayer but with stronger SOC for magnetic ions or anions. Their dynamic and thermal stability are confirmed by phonon dispersion (see Fig. S1 in the Supplemental Material [42]) and first-principles molecular-dynamics simulations (see Fig. S2 in the Supplemental Material [42]), respectively. Energy calculations of spin-spiral (see Fig. S3 in the Supplemental Material [42]) and Monte Carlo simulations (see Fig. S4 in the Supplemental Material [42]) confirm their ferromagnetic ground states and estimate their Curie temperature to be above room temperature except for the VTe₂ monolayer. The spin-induced polarization is significantly improved with respect to the VSe₂ monolayer [Fig. 1(f)]. The IP polarization of the RuBr₂ monolayer reaches up to 0.4 $\mu\text{C}/\text{cm}^2$, which is close to the polarization induced by the exchange-striction mechanism [45,46]. Therefore, this ferroelectric mechanism enables the coexistence and coupling of large spin-induced polarization and macroscopic magnetization above room temperature.

C. Spin-direction-dependent ferrovalley

Ferrovalley may also arise in 2D ferromagnets lacking inversion symmetry, where the combination of intrinsic exchange interaction and SOC leads to spontaneous valley polarization [8]. Similar to conventional valley materials, the VSe₂ monolayer shows valley-selective circular dichroism independent of SOC (see Fig. S5 in the Supplemental Material [42]). However, it has an IP magnetization (see Fig. S6 in the Supplemental Material [42]), resulting in the disappearance of spontaneous valley polarization. When the spin is along the OP direction, the valence-band maximum (VBM) and conduction-band minimum (CBM) between the two valleys are no longer equal, i.e., valley splitting occurs (see Fig. S7 in the Supplemental Material [42]). Figure 2(a) shows the energy variation of the highest occupied valence band in the whole Brillouin zone caused

by the change of spin direction from IP to OP. The maximum and minimum values of the energy variation appear at two valleys, K_+ and K_- , respectively, with opposite signs and unequal magnitudes. The valley splitting in both the VBM and the CBM exhibits spin-direction dependence [Fig. 2(b)], which arises from the first-order and second-order perturbation effects of SOC, respectively (see the Supplemental Material [42]). This results in a difference between the band gaps of the two valleys depending on the spin direction, i.e., proportional to the OP spin component.

The Berry-phase effect associated with the Bloch electrons is known to cause valley-contrasting physics, such as the valley Hall effect [6,7]. In the presence of an IP electric field, an electron will acquire an anomalous velocity in the transverse direction proportional to the Berry curvature. The Berry curvature has opposite signs at the two valleys (see Fig. S8 in the Supplemental Material [42]), causing electrons from the two valleys to deflect toward opposite boundaries. Due to the dependence on the optical band gap, the Berry curvature of the two valleys varies with the spin direction similarly to the valley splitting and the difference in their magnitudes is proportional to the OP spin component [Fig. 2(c)].

The combination of spin-induced ferroelectricity and the Berry-curvature effect can lead to fascinating physical phenomena, such as anomalous Hall conductivity dependent on the spin direction and the valley Hall effect without external electric field. The anomalous Hall conductivity, derived from the summation of the Berry curvature of the occupied states in the Brillouin zone [6], is also proportional to the OP spin component (see Fig. S9 in the Supplemental Material [42]). In addition, the voltage generated by the polarized charge may be superimposed onto the Hall voltage, causing the measured Hall voltage to depend on the spin direction. More interestingly, even in the absence of an external electric field, electrons and holes excited by circularly polarized light generate current along the internal electric field induced by the polarized charge, while the Berry-curvature effect leads to transverse charge and spin currents, as shown in Fig. 2(d).

D. Magnetoelectric cross control

A spin-Hamiltonian model including electric and magnetic field terms,

$$H = - \sum_{ij} J_{ij} \mathbf{S}_i \cdot \mathbf{S}_j - \sum_i K (S_i^z)^2 - \sum_i g \mu_B \mathbf{B} \cdot \mathbf{S}_i - \sum_i \mathbf{E} \cdot \mathbf{P}_i(\mathbf{S}_i) + \sum_{ij} \frac{C}{r_{ij}^3} \left[\mathbf{S}_i \cdot \mathbf{S}_j - \frac{3(\mathbf{S}_i \cdot \mathbf{r}_{ij})(\mathbf{S}_j \cdot \mathbf{r}_{ij})}{r_{ij}^2} \right], \quad (6)$$

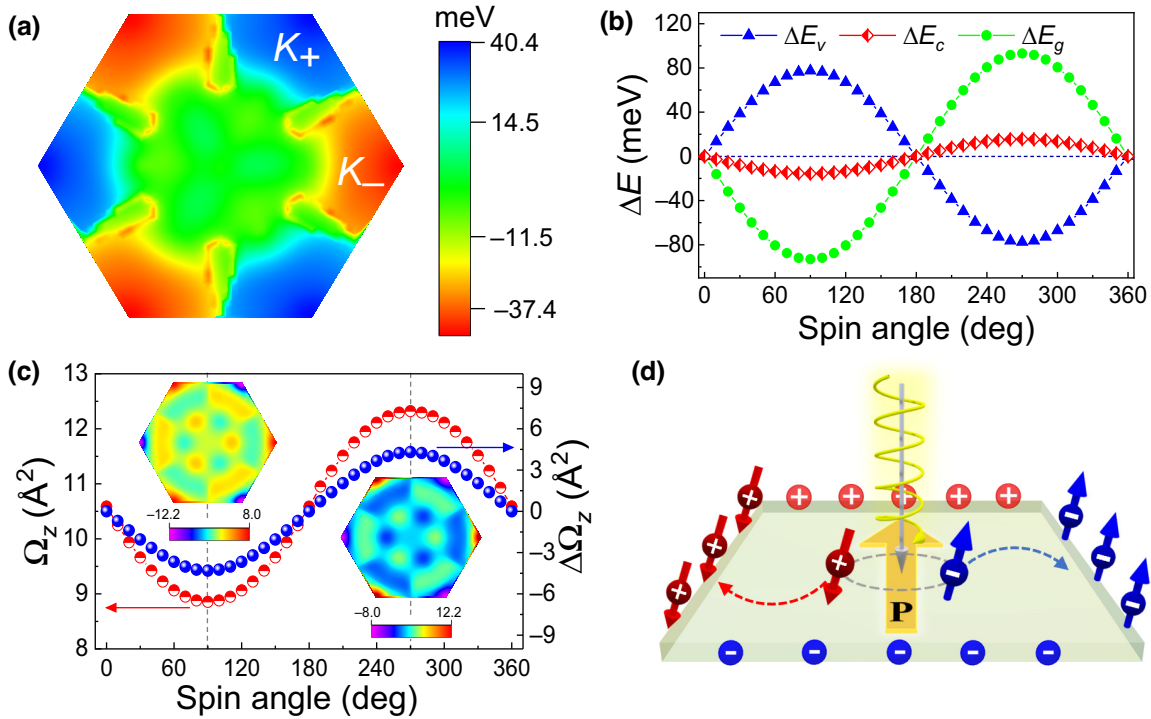


FIG. 2. The spin-direction-dependent ferrovalley and anomalous valley Hall effect without an external electric field. (a) The energy change of the highest occupied valence band of the VSe_2 monolayer in the whole Brillouin zone caused by the change of spin direction from IP to OP. (b) Valley splitting in the valence-band maximum (VBM) (ΔE_v), the conduction-band minimum (CBM) (ΔE_c), and the optical band gap (ΔE_g), each as a function of the spin angle. The spin angle represents the angle between the spin and the a - b plane. (c) The Berry curvature of a single valley and its magnitude difference between the two valleys as a function of the spin angle. The insets show the distribution of the Berry curvature in the Brillouin zone with the spin along the $+z$ and $-z$ axes, respectively. (d) A schematic of the anomalous valley Hall effect without an external electric field.

was used to study the control of polarization and magnetization by the external field, where \mathbf{S}_i and \mathbf{S}_j are the classical spin vectors at sites i and j , J_{ij} and K are the Heisenberg exchange interaction and single-ion anisotropy constant, respectively, and g and μ_B denote the Lande factor and Bohr magneton, respectively. $\mathbf{P}_i(\mathbf{S}_i)$ represents the local electric dipole moment induced by the single spin \mathbf{S}_i . The last term represents the dipole-dipole interaction, where $C = \mu_0(g\mu_B)^2/4\pi$ is a constant and \mathbf{r}_{ij} is the vector connecting sites i and j . The time evolution of the spin is described by the LLG equation.

Figure 3(a) shows the variation of the magnetization component of the VSe_2 monolayer with the magnitude of the magnetic field applied along the y axis. The initial magnetization is oriented along the IP direction at an angle of -60° to the x axis, due to the easy-plane magnetocrystalline anisotropy and the shape anisotropy caused by the demagnetizing field. The IP magnetization and polarization components change dramatically when the applied magnetic field reaches about 0.06 T. With the further increase of the magnetic field, the magnetization component M_x gradually reduces while M_y approaches saturation, i.e., the magnetization is close to parallel to the

magnetic field. This results in an increase and decrease in the magnitude of the polarization components P_x and P_y , respectively, indicating that the polarization is gradually approaching the $-x$ direction. When an OP magnetic field is applied, the M_z component increases linearly with the magnetic field, while the IP magnetization components decrease gradually [Fig. 3(b)]. The magnetization changes to the z -axis direction when the magnetic field exceeds approximately 20 T. The induced polarization components gradually reduce and disappear when the critical magnetic field is exceeded.

When an IP electric field is applied along the x axis, the polarization component P_x increases and approaches saturation with an increasing electric field, while the P_y component is gradually suppressed [Fig. 3(c)]. The change in polarization results from the transition of the spin direction toward the x axis. Applying an electric field along the $-y$ axis causes a similar transition of the polarization, i.e., it eventually turns to a direction parallel to the electric field [Fig. 3(c)]. Correspondingly, the spin is stabilized to the $[110]$ direction by the increasing electric field.

Figure 3(d) shows the dependence of the spin direction on the IP electric field direction under different field

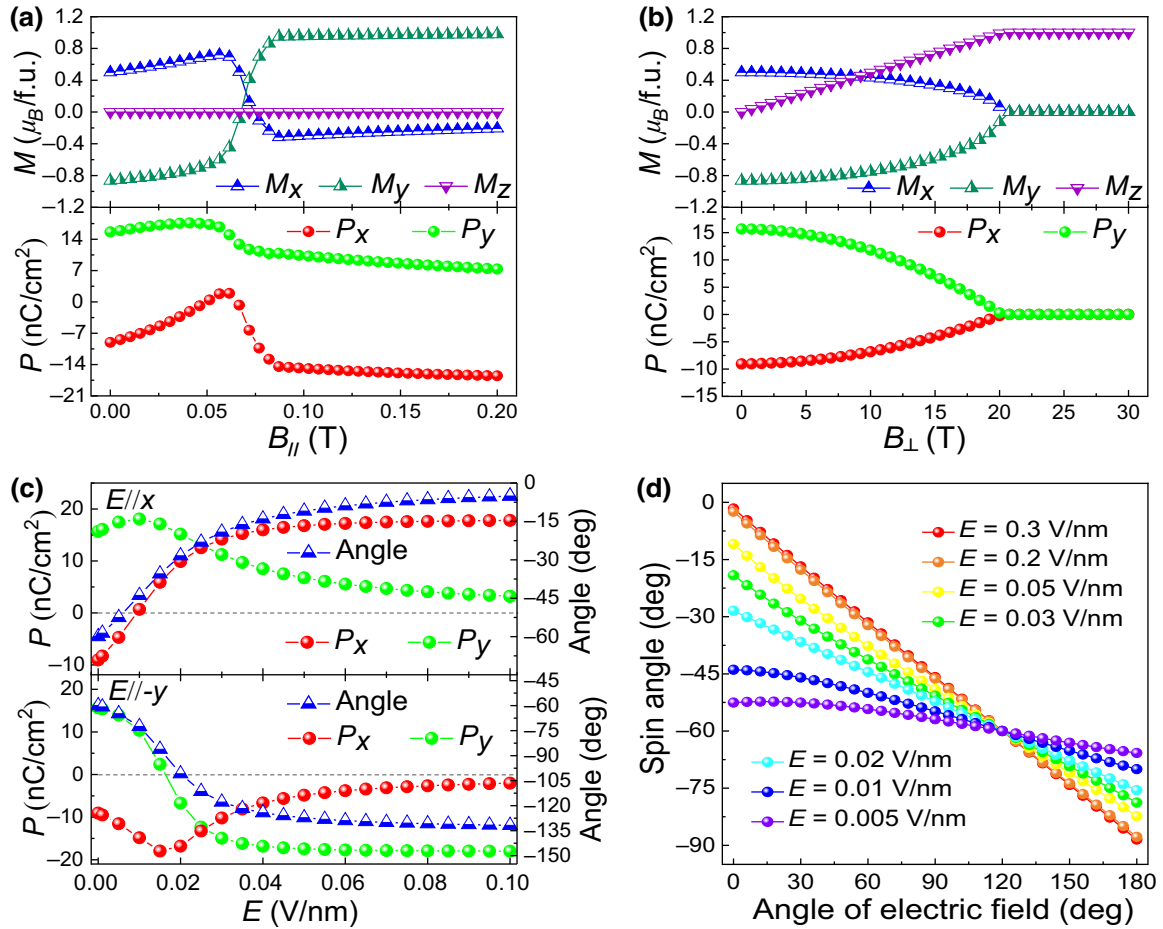


FIG. 3. The control of magnetization and electric polarization by magnetic and electric fields. The variation of the magnetization and polarization components of the VSe₂ monolayer with (a) IP (\mathbf{B}/y) and (b) OP (\mathbf{B}/z) magnetic fields, respectively: f.u., formula units. (c) The variation of the polarization components and the spin angle with an applied electric field along the x (upper) and $-y$ axes (lower), respectively. The spin angle refers to the angle of the average magnetization with respect to the x axis. (d) The variation of the spin angle with the direction of the IP electric field under different field strengths.

strengths. At small electric fields, the spin angle varies nonlinearly with the direction angle of the electric field and the coupling relationship depends on the strength of the electric field. However, at a large enough electric field, such as 0.2 V/nm, it becomes completely linear, following the rule $\theta_S = -1/2\theta_E$, where θ_S and θ_E are the direction angles of the spin and electric field, respectively. This is due to the fact that the spin-induced polarization, the direction angle of which is twice the spin angle, would be parallel to an electric field with a sufficiently large field strength.

At present, 2D multiferroics with the coexistence of ferroelectricity and ferromagnetism have been predicted in some van der Waals materials but few of them exhibit intrinsic magnetoelectric coupling effects [47,48]. Alternative routes such as constructing multiferroic heterostructures or multilayers with sliding ferroelectricity have been

proposed; however, their magnetoelectric coupling stems from weak interfacial effects [49–52]. Ferrovalley usually originates from the coupling effect of valley polarization with ferromagnetic and ferroelectric order parameters. The former is commonly found in 2D ferromagnetic semiconductors with a hexagonal lattice and OP magnetization, while the latter may arise in ferroelectrics the two valleys of which are symmetrically correlated by the crystal symmetry operator [20,53]. Although the desired electric field control of the valley can be achieved in the latter, it does not exhibit the physical effects associated with Berry curvature. The spin-induced ferroelectricity and magnetoelectric coupling effect discovered in this work enable the coexistence and coupling of three ferroics based on different electronic degrees of freedom in single-phase 2D materials and can be extended to other lattice systems, as depicted in Fig. 4.

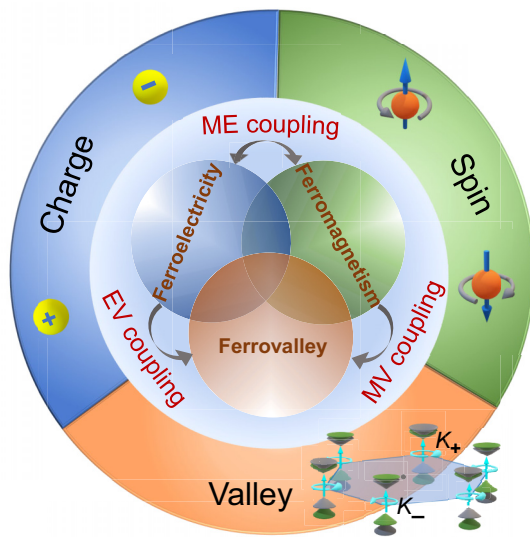


FIG. 4. The coexistence and coupling of various ferroics based on different electronic degrees of freedom. The possible coupling effects include the magnetoelectric (ME) coupling and the coupling of the electric polarization or magnetization with the valley, denoted as EV and MV, respectively.

IV. CONCLUSIONS

In conclusion, we demonstrate the coexistence and coupling between ferroelectricity, ferromagnetism, and ferrovalley in the van der Waals monolayer system. Both ferroelectricity and ferrovalley arise from the combined effects of inversion symmetry breaking and SOC. Spin-induced ferroelectricity can be explained by the p - d hybridization mechanism involving SOC, in which the OP polarization component is derived from the higher-order perturbation effect of SOC. The magnetoelectric cross control can be achieved based on the spin-polarization coupling, involving controlling magnetization by an electric field and electric polarization by a magnetic field. This work provides a design for 2D multiferroics with intrinsic magnetoelectric coupling and may help to facilitate the cross fusion of spintronics and valleytronics.

ACKNOWLEDGMENTS

This work was financially supported by the National Natural Science Foundation of China (Grants No. 11974418, No. 12374097, and No. 11834002). The computer resources provided by the High Performance Computing Center of Nanjing University are gratefully acknowledged.

[1] A. V. Chumak, V. I. Vasyuchka, A. A. Serga, and B. Hillebrands, Magnon spintronics, *Nat. Phys.* **11**, 453 (2015).

- [2] J. R. Schaibley, H. Yu, G. Clark, P. Rivera, J. S. Ross, K. L. Seyler, W. Yao, and X. Xu, Valleytronics in 2D materials, *Nat. Rev. Mater.* **1**, 16055 (2016).
- [3] T. Jungwirth, X. Marti, P. Wadley, and J. Wunderlich, Antiferromagnetic spintronics, *Nat. Nanotechnol.* **11**, 231 (2016).
- [4] A. Fert, N. Reyren, and V. Cros, Magnetic skyrmions: Advances in physics and potential applications, *Nat. Rev. Mater.* **2**, 17031 (2017).
- [5] Y. Tokura, K. Yasuda, and A. Tsukazaki, Magnetic topological insulators, *Nat. Rev. Phys.* **1**, 126 (2019).
- [6] D. Xiao, W. Yao, and Q. Niu, Valley-contrasting physics in graphene: Magnetic moment and topological transport, *Phys. Rev. Lett.* **99**, 236809 (2007).
- [7] D. Xiao, G.-B. Liu, W. Feng, X. Xu, and W. Yao, Coupled spin and valley physics in monolayers of MoS₂ and other group-VI dichalcogenides, *Phys. Rev. Lett.* **108**, 196802 (2012).
- [8] W.-Y. Tong, S.-J. Gong, X. Wan, and C.-G. Duan, Concepts of ferrovalley material and anomalous valley Hall effect, *Nat. Commun.* **7**, 13612 (2016).
- [9] N. A. Spaldin and R. Ramesh, Advances in magnetoelectric multiferroics, *Nat. Mater.* **18**, 203 (2019).
- [10] D. Zhang, M. Shi, T. Zhu, D. Xing, H. Zhang, and J. Wang, Topological axion states in the magnetic insulator MnBi₂Te₄ with the quantized magnetoelectric effect, *Phys. Rev. Lett.* **122**, 206401 (2019).
- [11] L. Du, T. Hasan, A. Castellanos-Gomez, G.-B. Liu, Y. Yao, C. N. Lau, and Z. Sun, Engineering symmetry breaking in 2D layered materials, *Nat. Rev. Phys.* **3**, 193 (2021).
- [12] J. W. Huang, X. Duan, S. Jeon, Y. Kim, J. Zhou, J. Li, and S. Liu, On-demand quantum spin Hall insulators controlled by two-dimensional ferroelectricity, *Mater. Horiz.* **9**, 1440 (2022).
- [13] Z. L. He, W. H. Du, K. Y. Dou, Y. Dai, B. B. Huang, and Y. D. Ma, Ferroelectrically tunable magnetic skyrmions in two-dimensional multiferroics, *Mater. Horiz.* **10**, 3450 (2023).
- [14] K. Chang, J. Liu, H. Lin, N. Wang, K. Zhao, A. Zhang, F. Jin, Y. Zhong, X. Hu, W. Duan, Q. Zhang, L. Fu, Q.-K. Xue, X. Chen, and S.-H. Ji, Discovery of robust in-plane ferroelectricity in atomic-thick SnTe, *Science* **353**, 274 (2016).
- [15] F. Liu, L. You, K. L. Seyler, X. Li, P. Yu, J. Lin, X. Wang, J. Zhou, H. Wang, H. He, S. T. Pantelides, W. Zhou, P. Sharma, X. Xu, P. M. Ajayan, J. Wang, and Z. Liu, Room-temperature ferroelectricity in CuInP₂S₆ ultrathin flakes, *Nat. Commun.* **7**, 12357 (2016).
- [16] W. Ding, J. Zhu, Z. Wang, Y. Gao, D. Xiao, Y. Gu, Z. Zhang, and W. Zhu, Prediction of intrinsic two-dimensional ferroelectrics in In₂Se₃ and other III₂-VI₃ van der Waals materials, *Nat. Commun.* **8**, 14956 (2017).
- [17] C. Gong, L. Li, Z. L. Li, H. W. Ji, A. Stern, Y. Xia, T. Cao, W. Bao, C. Z. Wang, Y. Wang, Z. Q. Qiu, R. J. Cava, S. G. Louie, J. Xia, and X. Zhang, Discovery of intrinsic ferromagnetism in two-dimensional van der Waals crystals, *Nature* **546**, 265 (2017).
- [18] B. Huang, G. Clark, E. Navarro-Moratalla, D. R. Klein, R. Cheng, K. L. Seyler, D. Zhong, E. Schmidgall, M. A. McGuire, D. H. Cobden, W. Yao, D. Xiao, P. Jarillo-Herrero, and X. Xu, Layer-dependent ferromagnetism in a

- van der Waals crystal down to the monolayer limit, *Nature* **546**, 270 (2017).
- [19] M. Bonilla, S. Kolekar, Y. Ma, H. C. Diaz, V. Kalappattil, R. Das, T. Eggers, H. R. Gutierrez, M.-H. Phan, and M. Batzill, Strong room-temperature ferromagnetism in VSe₂ monolayers on van der Waals substrates, *Nat. Nanotechnol.* **13**, 289 (2018).
- [20] X.-W. Shen, W.-Y. Tong, S.-J. Gong, and C.-G. Duan, Electrically tunable polarizer based on 2D orthorhombic ferrovalley materials, *2D Mater.* **5**, 011001 (2017).
- [21] J. J. Zhang, L. F. Lin, Y. Zhang, M. H. Wu, B. I. Yakobson, and S. Dong, Type-II multiferroic Hf₂VC₂F₂ MXene monolayer with high transition temperature, *J. Am. Chem. Soc.* **140**, 9768 (2018).
- [22] J. T. Zhang, X. F. Shen, Y. C. Wang, C. Ji, Y. Zhou, J. L. Wang, F. Z. Huang, and X. M. Lu, Design of two-dimensional multiferroics with direct polarization-magnetization coupling, *Phys. Rev. Lett.* **125**, 017601 (2020).
- [23] J. T. Zhang, Y. Zhou, F. Wang, X. F. Shen, J. L. Wang, and X. M. Lu, Coexistence and coupling of spin-induced ferroelectricity and ferromagnetism in perovskites, *Phys. Rev. Lett.* **129**, 117603 (2022).
- [24] C. Tang, L. Zhang, S. Sanvito, and A. J. Du, Enabling room-temperature triferroic coupling in dual transition-metal dichalcogenide monolayers via electronic asymmetry, *J. Am. Chem. Soc.* **145**, 2485 (2023).
- [25] X. F. Shen, F. Wang, X. M. Lu, and J. T. Zhang, Two-dimensional multiferroics with intrinsic magnetoelectric coupling in *A*-site ordered perovskite monolayers, *Nano Lett.* **23**, 735 (2023).
- [26] N. D. Mermin and H. Wagner, Absence of ferromagnetism or antiferromagnetism in one- or two-dimensional isotropic Heisenberg models, *Phys. Rev. Lett.* **17**, 1133 (1966).
- [27] A. Manchon, H. C. Koo, J. Nitta, S. M. Frolov, and R. A. Duine, New perspectives for Rashba spin-orbit coupling, *Nat. Mater.* **14**, 871 (2015).
- [28] D. Dai, H. Xiang, and M.-H. Whangbo, Effects of spin-orbit coupling on magnetic properties of discrete and extended magnetic systems, *J. Comput. Chem.* **29**, 2187 (2008).
- [29] P. E. Blöchl, Projector augmented-wave method, *Phys. Rev. B* **50**, 17953 (1994).
- [30] G. Kresse and J. Furthmüller, Efficient iterative schemes for *ab initio* total-energy calculations using a plane-wave basis set, *Phys. Rev. B* **54**, 11169 (1996).
- [31] S. L. Dudarev, G. A. Botton, S. Y. Savrasov, C. J. Humphreys, and A. P. Sutton, Rotationally invariant approach of Coulomb repulsion parameter *U*, *Phys. Rev. B* **57**, 1505 (1998).
- [32] E. Şaşıoğlu, C. Friedrich, and S. Blügel, Effective Coulomb interaction in transition metals from constrained random-phase approximation, *Phys. Rev. B* **83**, 121101 (2011).
- [33] R. D. King-Smith and D. Vanderbilt, Theory of polarization of crystalline solids, *Phys. Rev. B* **47**, 1651 (1993).
- [34] R. F. L. Evans, W. J. Fan, P. Chureemart, T. A. Ostler, M. O. A. Ellis, and R. W. Chantrell, Atomistic spin model simulations of magnetic nanomaterials, *J. Phys.: Condens. Matter.* **26**, 103202 (2014).
- [35] Y. Tokura, S. Seki, and N. Nagaosa, Multiferroics of spin origin, *Rep. Prog. Phys.* **77**, 076501 (2014).
- [36] E. Bousquet and A. Cano, Non-collinear magnetism in multiferroic perovskites, *J. Phys. Condens. Matter.* **28**, 123001 (2016).
- [37] X. Jiang, Q. Liu, J. Xing, N. Liu, Y. Guo, Z. Liu, and J. Zhao, Recent progress on 2D magnets: Fundamental mechanism, structural design and modification, *Appl. Phys. Rev.* **8**, 031305 (2021).
- [38] X. Wang, D. Li, Z. Li, C. Wu, C.-M. Che, G. Chen, and X. Cui, Ferromagnetism in 2D vanadium diselenide, *ACS Nano* **15**, 16236 (2021).
- [39] M. Matsumoto, K. Chimata, and M. Koga, Symmetry analysis of spin-dependent electric dipole and its application to magnetoelectric effects, *J. Phys. Soc. Jpn.* **86**, 034704 (2017).
- [40] H. J. Xiang, E. J. Kan, Y. Zhang, M.-H. Whangbo, and X. G. Gong, General theory for the ferroelectric polarization induced by spin-spiral order, *Phys. Rev. Lett.* **107**, 157202 (2011).
- [41] J. T. Zhang, C. Ji, J. L. Wang, W. S. Xia, B. X. Guo, X. M. Lu, and J. S. Zhu, Spin-induced ferroelectricity in a triangular-lattice antiferromagnet studied by magnetoelectric coupling tensors, *Phys. Rev. B* **96**, 235136 (2017).
- [42] See the Supplemental Material at <http://link.aps.org/supplemental/10.1103/PhysRevApplied.20.064011> for derivation of the expressions for spin-induced polarization and valley splitting, phonon band structures, first-principles molecular simulations, the energy of the spiral spin order, Monte Carlo simulation, circular dichroism, magnetic anisotropy, projected band structures, Berry curvature, and anomalous Hall conductivity.
- [43] C. Jia, S. Onoda, N. Nagaosa, and J. H. Han, Bond electronic polarization induced by spin, *Phys. Rev. B* **74**, 224444 (2006).
- [44] H. Murakawa, Y. Onose, S. Miyahara, N. Furukawa, and Y. Tokura, Ferroelectricity induced by spin-dependent metal-ligand hybridization in Ba₂CoGe₂O₇, *Phys. Rev. Lett.* **105**, 137202 (2010).
- [45] K. Shimamoto, S. Mukherjee, N. S. Bingham, A. K. Suszka, T. Lippert, C. Niedermayer, and C. W. Schneider, Single-axis-dependent structural and multiferroic properties of orthorhombic RMnO₃ (*R* = Gd-Lu), *Phys. Rev. B* **95**, 184105 (2017).
- [46] A. Guazzi, F. P. Milton, V. P. Gastaldo, M. Verseils, A. J. Gualdi, D. von Dreifus, Y. Klein, D. Garcia, A. J. A. de Oliveira, P. Bordet, and E. Gilioli, Ferroelectricity in the 1 μC/cm² range induced by canted antiferromagnetism in (LaMn₃)Mn₄O₁₂, *Appl. Phys. Lett.* **115**, 152902 (2019).
- [47] X. Tang and L. Kou, Two-dimensional ferroics and multiferroics: Platforms for new physics and applications, *J. Phys. Chem. Lett.* **10**, 6634 (2019).
- [48] J. Chu, Y. Wang, X. Wang, K. Hu, G. Rao, C. Gong, C. Wu, H. Hong, X. Wang, K. Liu, C. Gao, and J. Xiong, 2D polarized materials: Ferromagnetic, ferrovalley, ferroelectric materials, and related heterostructures, *Adv. Mater.* **33**, 2004469 (2020).
- [49] C. Gong, E. M. Kim, Y. Wang, G. Lee, and X. Zhang, Multiferroicity in atomic van der Waals heterostructures, *Nat. Commun.* **10**, 2657 (2019).

- [50] Q. Pei, B. Z. Zhou, W. B. Mi, and Y. C. Cheng, Triferroic material and electrical control of valley degree of freedom, *ACS Appl. Mater. Interfaces* **11**, 12675 (2019).
- [51] X. Liu, A. P. Pyatakov, and W. Ren, Magnetoelectric coupling in multiferroic bilayer VS₂, *Phys. Rev. Lett.* **125**, 247601 (2020).
- [52] T. Zhang, X. Xu, B. Huang, Y. Dai, and Y. Ma, 2D spontaneous valley polarization from inversion symmetric single-layer lattices, *npj Comput. Mater.* **8**, 64 (2022).
- [53] H. Cheng, J. Zhou, W. Ji, Y. Zhang, and Y. Feng, Two-dimensional intrinsic ferrovalley GdI₂ with large valley polarization, *Phys. Rev. B* **103**, 125121 (2021).